

pubs.acs.org/joc Article

Electrosynthesis of a Biaurone by Controlled Dimerization of Flavone: Mechanistic Insight and Large-Scale Application

Seyyedamirhossein Hosseini, Bishnu Thapa, Maria J. Medeiros, Erick M. Pasciak, Michael A. Pence, Eric B. Twum, Jonathan A. Karty, Xinfeng Gao, Krishnan Raghavachari, Dennis G. Peters, and Mohammad S. Mubarak*



Cite This: J. Org. Chem. 2020, 85, 10658-10669



ACCESS

Metrics & More

Article Recommendations

Flavone

Reaction Coordinate

Supporting Information

ABSTRACT: The electrochemistry of flavone (1) has been carefully investigated at glassy carbon cathodes in dimethylformamide containing 0.10 M tetra-n-butylammonium tetrafluoroborate as supporting electrolyte. In this medium, a cyclic voltammogram for a reduction of 1 exhibits a reversible cathodic process ($E_{\rm pc}=-1.58~{\rm V}$ and $E_{\rm pa}=-1.47~{\rm V}$ vs SHE) that is followed by an irreversible cathodic peak ($E_{\rm pc}=-2.17~{\rm V}$ vs SHE). When water (5.0 M) is introduced into the medium, the first peak for 1 becomes irreversible ($E_{\rm pc}=-1.56~{\rm V}$ vs SHE), and the second (irreversible) peak shifts to $-2.07~{\rm V}$ vs SHE. Bulk electrolyses of 1 at $-1.60~{\rm V}$ vs SHE afford flavanone, 2'-hydroxychalcone, 2'-hydroxy-3-phenylpropionate, and two new compounds, namely (Z)-1,6-bis(2-hydroxyphenyl)-3,4-diphenylhex-3-ene-1,6-dione (D1) and (Z)-2,2'-(1,2-diphenylethene-1,2-bis(benzofuran-3(2H))-one) (D2), obtained in significant amounts, that were characterized by means of $^{1}{\rm H}$ and $^{13}{\rm C}$ NMR spectrometry as well as single-crystal X-ray diffraction. Along with the above findings, we have proposed a mechanism for the electroreduction of 1, which has been further corroborated by our quantum mechanical study.

■ INTRODUCTION

Flavonoids are biologically important molecules found in various natural sources, such as the extracts of citrus fruits. Some flavonoids (Scheme 1) exhibit significant anticancer and anti-inflammatory properties. 3-8

Among these flavonoids, aurone and biaurone are attractive subclasses due to their natural abundance and potent biological activity. 9-13 Furthermore, these compounds are interesting reagents for the synthesis of more complex structures such as spirocycles and benzofuroazepinones. Shown in Scheme 2 is the possible approach to form a biarouene. 18-21 To form an aurone, an oxidative intermolecular cyclization of 2'-hydroxychalcones or various condensation approaches has proven to be effective. Then an electroreductive dimerization or a radical-radical coupling reaction can be used to obtain the indicated biaurone. However, these synthetic methods are associated with numerous obstacles such as low yield, use of expensive catalysts, and low atom economy. 21-25 Furthermore, the use of flavone to form a biaroune, a process that involves opening a six-membered ring and its closure to form a fivemembered ring conjugated with a double bond and subsequent dimerization, has not yet been reported.

On the other hand, electrosynthesis of relatively complex molecules such as heterocycles has gained momentum in recent years. In comparison with conventional methods of synthesis, electrosynthesis features a selective, fast, and green alternative since catalysts and reagents required for the

reaction can be minimized by the use of proper electrochemical methodology and suitable electrode materials. ^{30,31} In this context, it is worth mentioning that electrosynthesis can be accomplished via the two alternative modes of constant-current or controlled-potential electrolysis. ³² Constant-current electrolysis is technically less challenging and offers a faster approach to the formation of certain molecules. However, this feature can come at the cost of low selectivity. Accordingly, controlled-potential electrolysis (CPE) is the method of choice for the synthesis of complex molecules where higher selectivity is desirable.

Based on the above discussion, we report herein the first successful one-pot electrosynthesis of a biaurone via application of CPE. We have thoroughly examined the electrochemistry of an ether moiety coupled with an α,β -unsaturated ketone group in N,N-dimethylformamide (DMF) containing 0.10 M TBABF₄ with the aid of cyclic voltammetry and controlled-potential (bulk) electrolysis. Furthermore, we have investigated the effect of several proton donors on the reaction yield and product distribution. For each electrolysis,

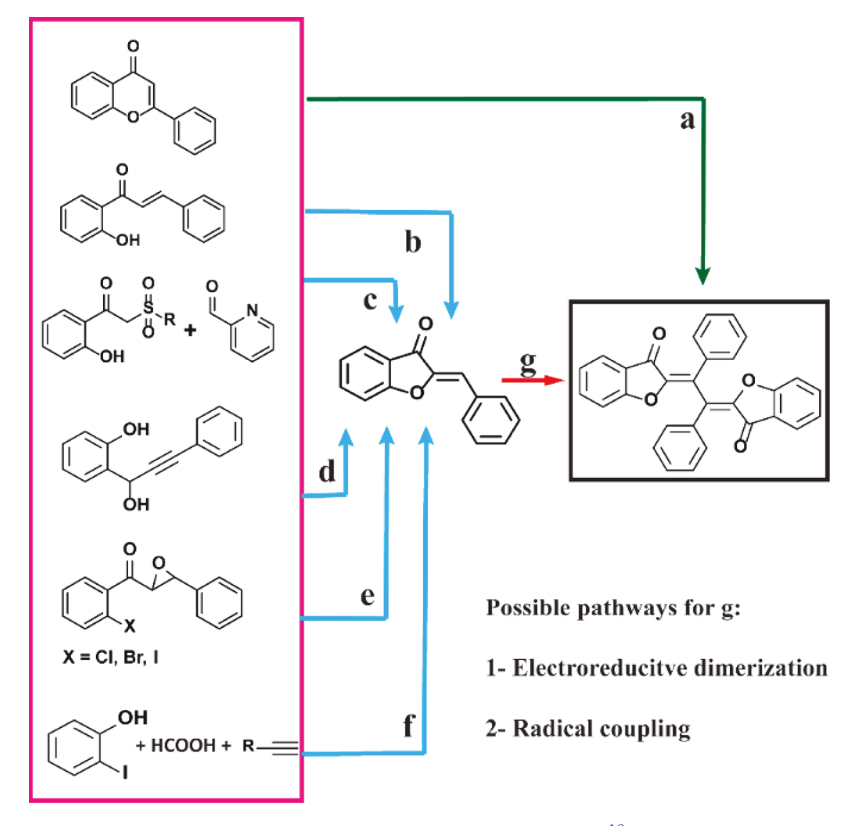
Received: May 20, 2020 Published: July 20, 2020





Scheme 1. Pharmaceutically Important Derivatives of Flavone

Scheme 2. Possible Synthesis of Biaroune from Various Starting Materials^a



"Including (a) present work (TBABF₄–DMF/water (10%), E = -1.10 V), (b) Yatabe et al. (O₂, Au–Pd catalyst immobilized onto CeO₂), (c) Cheng et al. (piperidine, HOAC, benzene), (d) Harkat et al. (AuCl, K₂CO₃, MeCN), (e) Weng et al. (CuI, 1,10-phenanthroline, Cs₂CO₃, 105 °C, N₂), (f) Qi et al. (Pd(PPh₃)₄, Et₃N, Ac₂O, toluene, 80 °C).

components of the mixture were separated employing normal-phase liquid chromatography, and each separated species was characterized with the aid of gas chromatography—mass spectrometry (GC-MS), high-performance liquid chromatography—electrospray ionization—mass spectrometry (HPLC-ESI-MS), and NMR spectroscopy. Finally, we have used

NMR spectroscopy and single-crystal X-ray diffraction data to establish the molecular structure of the target biaurone.

■ RESULTS AND DISCUSSION

Cyclic Voltammetric Studies. Displayed in Figure 1 are cyclic voltammograms obtained at 100 mV s⁻¹ for reduction of

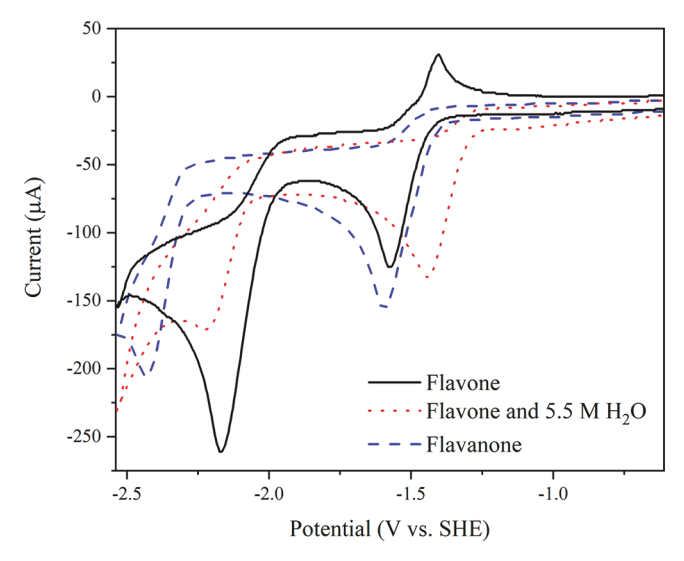


Figure 1. Cyclic voltammograms recorded at 500 mV s⁻¹ for reduction of 5.0 mM flavone at a glassy carbon electrode (area = $0.071~\rm cm^2$) in DMF containing 0.10 M TBABF₄. Black voltammogram (unbroken line) shows behavior in the absence of added water, red dotted voltammogram shows behavior in the presence of 5.5 M added water, and blue dashed trace shows electrochemical behavior of the flavanone (2) in absence of water. Each scan goes from $-0.50~\rm to$ $-2.50~\rm to$ $-0.50~\rm V$ vs SHE.

5.0 mM flavone (1, Scheme 4) or flavanone (2, Scheme 4) in DMF containing 0.10 M TBABF₄ at a glassy carbon cathode. Flavone exhibits a quasi-reversible redox couple ($E_{\rm pc}=-1.58$ V and $E_{\rm pa}=-1.47$ V vs SHE) (S24–S26 and Table S2) that is followed by an irreversible cathodic peak ($E_{\rm pc}=-2.07$ V vs SHE). Upon addition of an excess of water to the solution of 1 (dotted red trace), the potential of both cathodic peaks shifts to a less negative value. Additionally, the corresponding anodic peak (at -1.47 V) disappeared. Moreover, integration of the area under each cathodic peak revealed that the first redox couple involves a one-electron transfer, whereas the second peak corresponds to a two-electron reduction process.

Controlled-Potential (Bulk) Electrolyses of Flavone (1). Bulk electrolyses of flavone at potentials corresponding to the first cathodic peak in the presence of an added proton donor led to the formation of several products. As shown in Table 1, the amounts of unreacted flavone as well as products D1 and D2 (structures are shown in Scheme 4) increase as pK_a of the proton donor increases. However, the use of a less potent proton donor leads to the formation of lower yields of

flavanone and compounds 3 and 4 (structures displayed in Scheme 4).

Products D1 and D2 were crystallized through a slow solvent-evaporation method (see Supporting Information). Both samples (D1 and D2) were characterized by single-crystal X-ray diffraction (Figure S1-S4), high-resolution mass spectrometry, as well as NMR spectroscopy (Figure S5-S14). Compound D1 is a linear hydrodimer of 4 with a $P2_1/n$ space group, whereas D2 has the structure of a biaurone, which is a cyclized hydrodimer whose crystal structure belongs to the pbca space group. However, differences in the molecular structures of D1 and D2 rule out the possibility of intermolecular conversion of these two species. Further electrochemical studies were performed on D1 and D2 to confirm the validity of this hypothesis. We further probed the role of proton donors on the yield of the biaurone (D2) by varying the water concentration in the supporting electrolyte (Table 2). Data in Table 2 revealed that the yield of D2

Table 2. Coulometric Data and Product Distributions for Controlled-Potential (Bulk) Electrolyses of 5.0 mM Flavone (1) at Reticulated Vitreous Carbon Cathodes Held at -1.60 V vs SHE in DMF Containing 0.10 M TBABF $_4$ and an Excess of Water

entry	$[H_2O](M)$	n^a	D1 to D2 ratio
1	0.10	3.10	1.8:1
2	1.10	3.31	1:1
3	2.10	3.52	1:1.2
4	5.50	3.71	1:1.8
5	8.10	3.71	1:1.8

^aAverage number of electrons transferred per molecule of flavone (1).

increases with increasing proton-donor concentration. However, with water concentrations above 5.50 M, no significant change either in yield or product ratio was observed. Based on these results, we conclude that the optimal condition to produce compound **D2** is to use a flavone-to-proton donor ratio of 1:1000.

Proton-Donor Effect. As shown by the previous results, the electrochemical behavior of the flavone is greatly influenced by the nature and concentration of the proton donor. When water was employed at the optimal concentration (5.5 M), two surprising products, including **D1** and **D2**, were formed. Electrochemistry of enones has been the subject of several publications. Enones exhibit two cathodic peaks roughly around -0.90 and -1.70 V vs SHE in the absence of proton donors (a sample electrochemical behavior of these

Table 1. Coulometric Data and Product Distributions for Controlled-Potential (Bulk) Electrolyses of 5.0 mM Flavone (1) at Reticulated Vitreous Carbon Cathodes Held at -1.60 V vs SHE in DMF Containing 0.10 M TBABF₄

				product distribution ^a (mol. %)					
entry	proton donor	pK_a	n^{b}	1	2	3	4	D1 ^e	D2 ^e
1	CH ₃ COOH	13.36	2.50	trace	50	23	25	trace	trace
2	$HFIP^c$	18.8	2.10	4	11	41	18	15 (3.2 mg)	8 (1.8 mg)
3	H_2O	32.2	3.06	11	3	7	12	23 (4.9 mg)	42 (9.7 mg)
4^d	H_2O	32.2	4.12	25	6	7	9	16 (3.4 mg)	35 (8.1 mg)

^a1 = flavone, 2 = flavanone, 3 = 2'-hydroxychalcone, 4 = 2'-hydroxy-3-phenylpropionate, D1 = 1,6-bis(2-hydroxyphenyl)-3,4-diphenylhexane-1,6-dione, D2 = (Z)-2,2'-(1,2-diphenylethane-1,2-diyl)bis(benzofuran-3-(2H)-one). ^bAverage number of electrons per molecule of substrate. ^cHFIP = 1,1,1,3,3,3-hexafluoro-2-propanol. ^dControlled-potential electrolysis carried in the presence of adventitious oxygen. ^eNumbers in parentheses show yields in milligrams for electrosynthesis of D1 and D2.

molecules that bear the enon moiety is shown in Figure S27). It was shown that the first cathodic event is due to the reduction of the activated double bond that affords a radical anion (one electron process). The second peak arises from the reduction of the carbonyl group to form the corresponding alcohol (a two-electron process). However, for flavone (1), an ether group is coupled with the enone moiety; hence, the electrochemical nature of the first reduction peak may differ from that of α,β -unsaturated carbonyls (R₁CH = CHCOR₂). We carried a number of electrochemical studies to elucidate the underlying electrochemical mechanism of electron transfer in flavone.

Electrochemical behavior of flavone shows a close dependency on the concentration of water (Figure 2). In parallel with

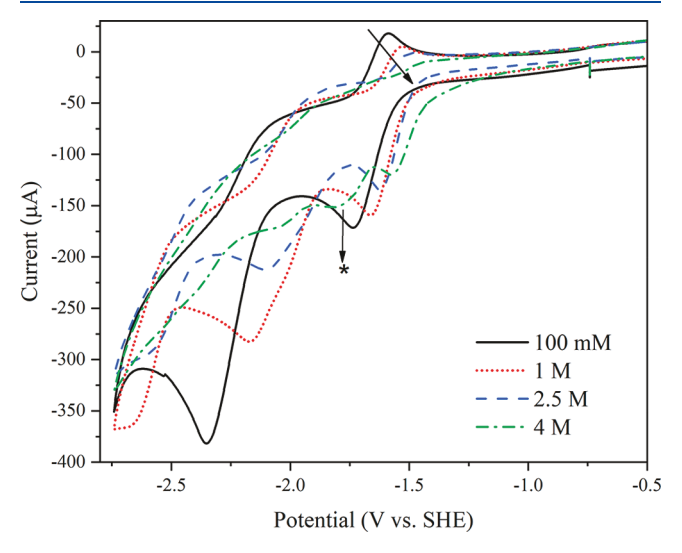


Figure 2. Cyclic voltammograms recorded for 5.0 mM flavone in the presence of various amount of water including 100 mM (solid black voltammogram), 1.0 M (dotted red line), 2.50 M (dashed blue line), and 4.0 M (dashed-dotted green trace) at a glassy carbon electrode (area = 0.071 cm²) in DMF containing 0.10 M TBABF₄. Secondary reduction peak, indicated with an asterisk, appears at water concentrations higher than 4.0 M. Height of the reversible oxidation peak declines in accordance with increasing water concentration as indicated by the diagonal arrow. Also, the first reduction peak shifts 160 mV with increasing water concentration, indicating dependency of the first peak on water concentration.

increasing water content of the supporting electrolyte, the reversibility of the redox peak at -1.50 V declines. Additionally, higher scan rates are needed to probe the oxidation peak (Figures S28 and S29). These observations confirm that the first peak at -1.50 V involves a slow reduction process and the rate of electrochemical process and stability of reduced species depends on the concentration of the proton donor. Also,

significant displacement of the cathodic peak position with changes in water concentration confirms that the reduction process involves a proton-coupled electron transfer reaction (i.e., 166 mV comparing peak positions with 100 mM and 4.0 M of added water). With respect to relative thermodynamic stability of the intermediates (S32), we believe the first reduction peak at -1.50 V involves formation 1a and 2b as shown in Scheme 3.

From a thermodynamic point of view, 2b is more stable than 1a; however, the standard reduction potential of these intermediates is well below -1.50 V (-0.44 V and -0.78 V respectively). Consequently, it is reasonable to assume that both of these intermediates can form, and possibly interconvert, under our working conditions.

Furthermore, in the presence of the optimal water concentrations (above 4.0 M) and slow scan rates (than 100 mV/s and slower), a new reduction peak at -1.75 V arises (Figure 2, peaks shown by an asterisk). The nature of this peak was examined with the aid of the slow scan rate studies (Figure 3). As the potential sweep rate decreases, the magnitude and

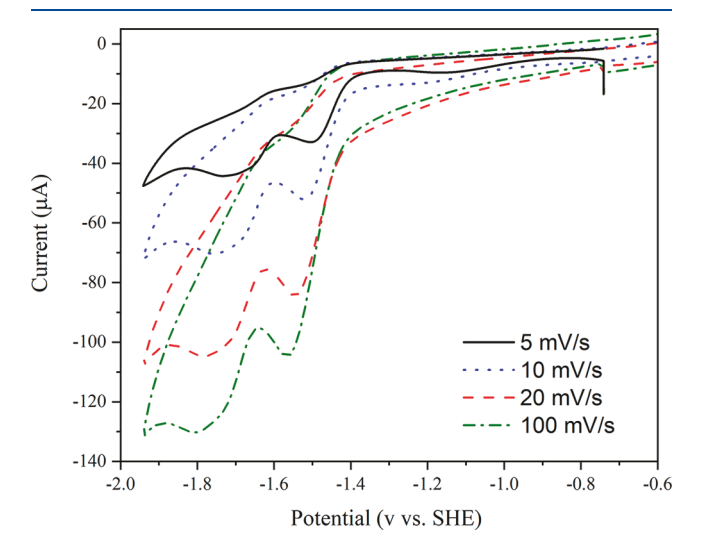


Figure 3. Cyclic voltammograms recorded for 5.0 mM flavone at 5 mV/s (solid black voltammogram), 10 mV/s (dotted blue line), 20 mV/s (dashed red trace), and 100 mV/s (dashed-dotted green trace) at a glassy carbon electrode (area = 0.071 cm²) in DMF containing 0.10 M TBABF $_4$ and 5.5 M water. Reversible oxidation peak appears at 1.0 V/s as a small peak starting from a scan rate of 500 mV/s.

the area under the new peak increase. Eventually, at scan rates slower than 10 mV/s, the area and the current for potential peaks located at -1.50 V and -1.75 V become comparable. As the result, we concluded that upon formation, 1a or 2b undergoes a slow chemical reaction to yield a new species that is reducible at potentials close to our working conditions.

Scheme 3. Reduction of Flavone at the First Cathodic Peak (-1.50 V vs SHE) in DMF-TBABF₄ (0.10 M) and in the Presence of Water at 4.0 M and Higher Concentrations

Scheme 4. Stepwise Mechanism for Electroreduction of Flavone in the Presence of a Proton Donor

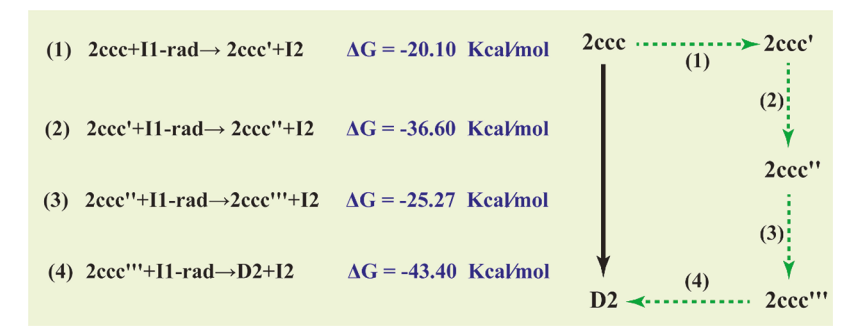
"Blue dashed lines show the reaction pathway in the presence of less potent proton donors, whereas the red dashed line represents electrolysis pathway in an acidic medium. 2 = flavanone, 3 = 2' - hydroxychalcone, 4 = 2' - hydroxy-3-phenylpropionate, D1 = 1,6 - bis(2 - hydroxyphenyl) - 3,4 - diphenylhexane-1,6-dione, D2 = (Z) - 2,2' - (1,2 - diphenylethane-1,2-diyl) bis(benzofuran-3-(2H) - one).

The electrochemical behavior of the flavone in the presence of a more potent proton donor including acetic acid and HFIP also shows the same lack of reversibility (Figure S30). Nevertheless, a much lower concentration is needed to carry out the same reduction process. Considerable cathodic potential shift and dependency of the electrochemical behavior to the pK_a of proton donor confirms that the reduction process has a PCET nature. Furthermore, electrolysis of flavone affords 3 and 4 once a more potent proton donor (i.e., acetic acid or HFIP) is employed. This observation confirms that the first reduction peak is a two-step process and includes (a) reduction of the conjugated double bond and (b) cleavage of ether moiety. With regard to the result of DFT analysis (see below), in the presence of the potent proton donor, the formation of 1a or 2b is followed rapidly by dissociation of the C-O bond, which then affords 3 and 4. These assumptions were further

confirmed by considering the electrochemical behavior of the flavanone (2). The only difference between the structure of 1 and 2 is the lack of the conjugated double bond between carbonyl and ether moieties. Cyclic voltammograms of flavanone show two irreversible reduction peaks at -1.50 and -2.51 V (Figure 1, blue dashed trace). Lack of reversible redox peak at -1.50 V confirms that reduction of flavanone involves cleavage of the ether moiety. Electrolysis of 2 at the optimal water concentration (above 4.0 M) and -1.50 V affords D1, which confirms the hypothesis about the sequential reduction mechanism that ultimately leads to the cleavage of the C–O bond.

Mechanistic Aspects of the Electroreduction of Flavone (1). Using a combination of experimental evidence and computational analysis with the B3LYP density functional theory (see the Supporting Information), we have proposed a

Scheme 5. Hydrogen Atom Abstraction via Electrogenerated Radicals^a



"Shown in the left panel is an example for reaction free energy of I2 radical intermediate and 2ccc. As indicated in the right panel, oxidation of 2ccc involves a sequential four-step reaction (shown by the dotted green arrow) to afford D2. Structures of 2ccc, 2ccc', 2ccc', and 2ccc'' are shown in S37. A complete list for HAT reaction free energies is shown in Figure S38.

mechanism for the electroreduction of flavone (Scheme 4). This mechanism accounts for the formation of the various electrolysis products obtained under different experimental conditions. It is important to note that most of the reaction steps involving an electron and proton transfer are discussed as a proton-coupled electron transfer (PCET) event to assess if the process is favorable with our applied electrochemical potential. However, since many of the reduction intermediates are highly unstable, one must consider the occurrence of a hydrogen-atom transfer (HAT) reaction or a competition between HAT and PCET events. According to Scheme 4 (i.e., S35), in the first step of electroreduction, 1 accepts an electron, which is followed by a proton transfer to form the key intermediate, 1a. In the presence of a weak proton donor such as water (indicated by dashed violet line), 1a undergoes isomerization to afford intermediate **2b** (ca. $\Delta G = +2.07$ kcal/ mol, P1) which further dimerizes to form I1 (ca. $\Delta G = -8.17$ kcal/mol). Next, in two consecutive steps, I1 accepts two electrons and two protons in total (i.e., two successive PCET processes) to yield I2. Both of these steps are calculated to be significantly favorable ($E_{PCET}^{o} = -0.05 \text{ V}$, and +1.61 V vs SCE, respectively) under our reaction conditions. We determined the structure of I2 with the aid of several spectroscopic techniques, including one- and two-dimensional NMR and high-resolution mass spectrometry (see Supporting Information Figures S15-S20). In the next step, I2 undergoes two favorable PCET reactions accepting two-electrons and two protons in a stepwise fashion to form D1.

Flavone can afford D2 by the reaction mechanism shown in P2 (Scheme 4, S36). In parallel to the reaction described above, 1a affords intermediate 2cc in a two-step reaction process involving the formation of an oxo-radical intermediate **2c−o** (ca. ΔG_{TS1} = +16.79 kcal/mol; $\Delta G_{1a\to 2c-o}$ = −2.04 kcal/ mol) which is followed by a ring-closure reaction (ca. ΔG_{TS2} = +15.43 kcal/mol; $\Delta G_{1a\rightarrow 2c-o} = -3.38$ kcal/mol). These two steps are computed to be significantly more favorable over the concerted pathway involving a six- to five-membered ring transformation ($\Delta G_{TS3} = +53.47 \text{ kcal/mol}$). Upon formation, 2cc can dimerize directly to afford a new species; however, we assume the intermediate 2cc undergoes a keto-enol tautomerization to afford more thermodynamically stable intermediate 2cco, which then dimerizes to give 2ccc (Figure S36). Transformation of 2ccc to D2 is a sequential oxidation reaction which may involve three intimidates including 2ccc', 2ccc", 2ccc" (Figure S37). We believe oxidation of the intermediate 2ccc under our working conditions can happen

via two concurrent pathways including (i) hydrogen atom abstraction by electrogenrated radicals and (ii) reactions with adventitious oxygen radicals in the catholyte.

As shown in Schemes 3 and 4, reduction of flavone affords a number of radical-bearing intermediates. Our analysis indicates that almost all of the electrogenerated radical intermediates can exothermically accept the hydrogen atom from 2ccc and its following intermediates to give D2 (Figure S38, $\Delta G_{\rm HAT}$ ranges from -34.99 to -10.28 kcal/mol). An example for hydrogenatom abstraction via electrogenerated radicals is shown in Scheme 5.

As mentioned earlier, another possibility for the oxidation of 2ccc to D2 involves participation of the adventitious oxygen. Cyclic voltammetry of oxygen in our working condition shows two reduction peak at -0.70 and -1.50 V (Figure S39). The second peak for reduction of oxygen matches well with the potential we employed to electrolyze flavone. An electrolysis was carried in the presence of the catalytic amount of the oxygen at -1.5 V to investigate the interaction of the reduced oxygen and flavone (Scheme 2, Supporting Information). Comparing with the controlled experiment (Table 1, entry 3), the amount of the unreacted flavone has increased from 10 to 25% when the electrolysis was carried out in the presence of oxygen (Table 1, entry 4). Furthermore, D2 still forms in a considerable amount, which confirms the involvement of adventitious oxygen. Finally, the *n*-value for this experiment is elevated, which can be attributed to direct oxygen reduction. However, increasing the ratio of oxygen, e.g., replacing the Ar stream with a stream of oxygen in the gas mixture, disrupts the electrolysis; a negligible amount of flavone electrolyzes to afford 2, and the electrolysis affords substantial amounts of

Reduction of flavone affords a number of stable intermediates; hence, it is possible to propose various reaction mechanisms to account for the appearance of D1 and D2. For example, one can argue that over-reduction of D2 can also afford D1. While we are unable to altogether reject this assumption, we believe this transformation is not likely to happen under our experimental conditions. This argument is also corroborated by our experimental observations. As mentioned earlier, we detected insignificant amounts of I2. However, electrolysis of I2 under our working conditions solely afforded D1, and no trace of D2 was found. Furthermore, purified D2 did not undergo a further reduction under our working conditions. These observations nullify, to a reasonable degree of confidence, the possibility of cross

Table 3. Product Distributions for Controlled-Potential (Bulk) Electrolyses of Various Concentrations of Flavone (1) at Reticulated Vitreous Carbon Cathodes Held at $-1.6~\rm V$ vs SHE in DMF Containing 0.10 M TBABF₄ and Water Concentration of 5.5 M

	product distribution b (wt %)					
[flavone] ^a	1	2	3	4	D1 ^c	D2 ^c
10 mM (44.53 mg)	11	3	7	12	23 (10.24 mg)	42 (18.70 mg)
30 mM (133.60 mg)	23	4	10	13	19 (25.38 mg)	31 (41.41 mg)
100 mM (445 mg)	34	5	11	13	15 (66.75 mg)	22 (97.91 mg)

"All experiments were carried out in a 20 mL electrolysis cell. "Products of the electrolysis were separated with the aid of the normal-phase chromatography and dried under vacuum, and the purity of each product was verified with the aid of H¹ NMR. The weight of purified resultant was divided by flavone to obtain the corresponding weight percent. "The amount of the electrosynthesized **D1** and **D2** in milligram are reported in parentheses.

transformation of D1 and D2. Furthermore, formation of the product D2 results from an oxidation, possibly involving a combination of hydrogen atom abstraction by intermediates in solution during the reaction and oxidation by oxygen radicals, either during the electrolysis or following the reaction. However, more work would need to be done to test the stability of 2ccc in order to gain a better understanding of this portion of the mechanism.

A shown in Table 1, flavanone forms in a wide range of proton donors. To account for this observation, we propose the step-by-step mechanism shown in P3. In the presence of a proton, 1a undergoes reduction (ca. $E^{\circ} = -1.47 \text{ V vs SCE}$) along with uptake of a proton or overall a PCET process to give flavanone (2, p $K_a = 44.91$; $E_{PCET}^{o} = +1.18 \text{ V}$). Once flavone is electrolyzed in the presence of HFIP or acetic acid, large amounts of flavanones 3 and 4 form. To account for this observation, we propose the detailed mechanism shown in P4 (Scheme 4). In the presence of a potent proton donor, 1a undergoes immediate protonation; this step then can lead to saturation of the conjugated double bond (formation of flavanone) or rapid ring opening to yield 3. Once formed, 3 acquires two electrons and two protons in two successive and favorable PCET steps ($E_{PCET}^{o} = -0.48 \text{ V}$, and +1.33 V vs SCE, respectively) to give 4 (S34). At a potential of -1.20 V vs SCE (i.e., - 1.60 V vs SHE), compound 4 is inactive and cannot undergo further reduction.

In conclusion, a number of pieces of evidence helped us to propose Scheme 4 to account for the product distribution reported in Table 2. These include but are not limited to (a) product distribution as a function of the strength and concertation of proton donor, (b) effect of proton donor concentration and strength on the reversibility of the first redox peak, (c) appearance of new redox peak and scan rate studies, and (d) thermodynamic stability of intermediates. As shown, nature and concentration of the proton donor can be utilized as a facile tool to control reactivity of the intermediate. In this context, dimers of **D1** and **D2** will form once flavone was electrolyzed in DMF-TBABF4 that includes large excess of water as the proton donor (4.0 M or above).

Gram-Scale Synthesis. To scale-up the electrosynthesis, we used higher concentrations of the starting materials, while the concentration of proton donor and supporting electrolyte remained the same as before. Figure 4 compares cyclic voltammograms for the reduction of 10, 30, and 100 mM of flavone. At 10 mM, cyclic voltammogram mimics those seen in Figure 1. However, at higher concentrations, the first two peaks merge to form a single irreversible reduction peak while the position of the third peak remains unchanged. Electrolyses at high concentrations were carried out at -1.60 V, and our

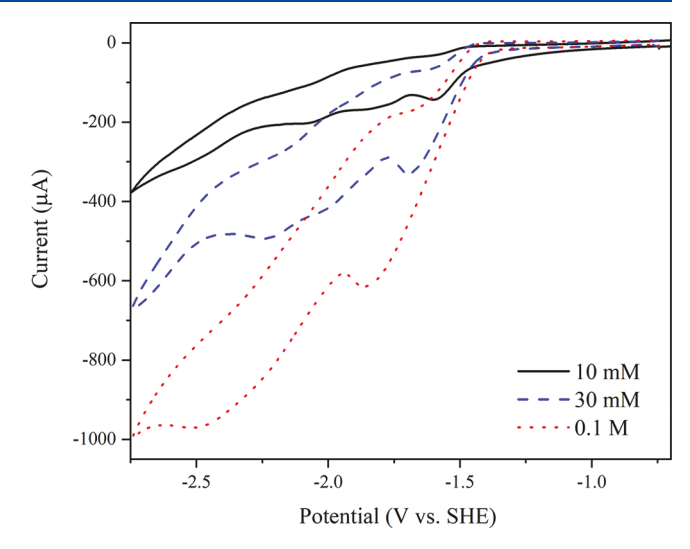


Figure 4. Cyclic voltammograms recorded at 100 mV s⁻¹ for reduction of flavone at a glassy carbon electrode (area = 0.071 cm^2) in DMF containing 0.10 M TBABF₄ in the presence of 5.5 M water. Black voltammogram (unbroken line) was obtained at 10 mM, blue trace (dashed line) shows the behavior of 30 mM of flavone, and dotted red trace represents electrochemical behavior of 1 at 0.1 M. Each scan goes from -0.50 to -2.50 to -0.50 V vs SHE.

analysis proved that with increasing flavone concentration the yield of reaction decreases (Table 3).

This could be due to the partial meltdown of the methylcellulose plug that separates the cathode and anode component, as electrolysis in higher concentration involves the passage of high current density. A meltdown of the permeable membrane will allow movement of reduced intermediates from the cathode compartment to anode where they will revert to their original form as the result of oxidation.

CONCLUSIONS

Electroreduction of flavone (1) at carbon cathodes in DMF containing 0.10 M TBABF₄ in the presence of various proton donors yields two new compounds in significant amounts: (Z)-1,6-bis(2-hydroxyphenyl)-3,4-diphenylhex-3-ene-1,6-dione (D1) and the naturally occurring biaurone (Z)-2,2'-(1,2-diphenylethene-1,2-bis(benzofuran-3(2H))-one) (D2). In the presence of a potent proton donor (1,1,1,3,3,3-hexafluoro-2-propanol), ring-opening from the ether terminal followed by protonation of a conjugated double bond is dominant. On the other hand, in the presence of a weak proton donor (water), dimerization dominates. More importantly, the optimization of the flavone-to-proton-donor ratio leads to the formation of

more of the natural product biaurone (D2). Additionally, electrodimerization of flavone can be carried out under mild experimental conditions at room temperature, and the extent of dimerization can be controlled by a change in the proton donor. Results from this investigation also revealed that, in the absence of an activated double bond (as in flavanone), reduction takes place through the ether moiety. Flavanone (2) undergoes dimerization when a weak proton donor (H₂O) is employed; however, in the presence of a potent proton donor (HFIP), reduction proceeds via ring-opening and subsequent hydrogenation.

■ EXPERIMENTAL SECTION

Reagents. Each of the following reagents (with commercial source and purity in parentheses) was used as received: dimethylformamide (DMF, EMD Millipore, 99.9%), methyl cellulose (Sigma-Aldrich, 95%), flavone (Sigma, Aldrich, 95%), flavanone (Sigma-Aldrich, 98%), 2'-hydroxychalcone (Alfa Aesar, 98%), 2-hydroxy-3-phenyl-propiophenone (TCI, > 98%). Tetra-n-butylammonium tetrafluoroborate (TBABF₄, GFS Chemicals, 98.5%), used as supporting electrolyte, was recrystallized from ethyl acetate—diethyl ether and stored under vacuum at 80 °C to remove traces of water. Deaeration of all solutions for cyclic voltammetry and controlled-potential (bulk) electrolyses were carried out with zero-grade argon (Air Products).

Cells, Electrodes, Instrumentation, and Procedures. Detailed information about cells, electrodes, instrumentation, and procedures for cyclic voltammetry and controlled-potential electrolysis are described in previous publications. ^{38–42} In summary, cyclic voltammograms were obtained with the aid of a Princeton Applied Research Corp. (PARC) model 2273 potentiostat–galvanostat operated by PowerSuite software. All potentials were measured experimentally with respect to a reference electrode consisting of a cadmium-saturated mercury amalgam in contact with DMF saturated with both cadmium chloride and sodium chloride; this electrode has a potential of –0.76 V versus the aqueous saturated calomel electrode (SCE) at 25 °C. ^{43,44} However, all potentials cited in this paper are given with respect to the standard hydrogen electrode (SHE).

All constant-potential electrolyses were carried out in a divided cell in which anode and cathode compartments are separated via a permeable membrane made of methyl cellulose and DMF. The cathode compartment hosts the reference electrode, gas inlet, gas outlet, and a working electrode. The anode section comprises a graphite rode submerged in oxygen-free DMF-TBAB4, and the bottom of the anode is filled with the permeable membrane. Prior to each electrolysis, the catholyte was deoxygenated by the introduction of a stream of Ar (Airgas, 99.99% purity grade) while stirred vigorously. After complete deoxygenation, a desirable potential is applied, which is marked by a negligible current spike (A in Figure S31). Once the initial current spike decayed to the background level, flavone (22.22 mg for a 5 mM electrolysis) was dissolved in 2 mL of deaerated catholyte and injected at once into the cathode compartment. This stage is accompanied by a marked current spike that is shown by B in Figure S31. During the electrolysis, a stream of Ar remained uninterrupted to prevent diffusion of oxygen into the electrolysis mixture. Similar protocol was carried out for electrolyses at higher concentrations of flavone. Controlled-potential (bulk) electrolyses were performed with the aid of a PARC model 173 potentiostat. A locally written LabView program was used for the collection of data, which were processed with OriginPro 2018 software.

Separation, Identification, and Quantitation of Products. At the end of each controlled-potential electrolysis, the catholyte was hydrolyzed with 1.6 M HCl, extracted into 60 mL of ethyl acetate, and finally washed in succession with three 35 mL portions of brine and 35 mL of water. Then the organic phase was dried over anhydrous sodium sulfate, and the solvent was evaporated under reduced pressure. Finally, components of the concentrated organic phase were separated by application of normal-phase chromatography. For this

mean, concentrated organic phase load onto a silica (50 μ m) and eluted with a programmed mobile phase. Normal phase chromatography was carried out with application of a Combiflash NextGen300+ (Teledyne Isco) equipped with a fraction collector. Elution was monitored at two wavelentghe of λ = 254 nm and λ = 280 nm. Typical chromatograms for separation of product mixture and further purification of **D1** and **D2** are shown in the Supporting Information (S21–S23). Finally, separated fractions were dried under vacuum at 70 °C, and the amount of the electrosynthesized sample has been measured by weighting the dried material. For all products, the yield of the reaction is shown as mol % (Table 1) and weight % (Table 2). Products of the reaction were identified by means of gas chromatography—mass spectrometry (GC—MS), various forms of NMR spectroscopy, HRMS measurements, and single-crystal X-ray diffraction analysis.

NMR spectra were acquired on a 500 MHz Varian Inova spectrometer with tetramethylsilane (TMS) as an internal standard. Chemical shifts are expressed in δ units, and $^1\mathrm{H}-^1\mathrm{H}$ coupling constants are given in hertz. GC–MS studies were conducted with a Hewlett–Packard 6890N gas chromatograph, fitted with a 30 m \times 0.25 mm i.d. Agilent DB-5 capillary column and coupled to a Hewlett-Packard model 5973 inert mass-selective detector operating in electron–ionization mode (70 eV). HRMS measurements were carried out with the aid of a Hewlett–Packard 5890 Series II gas chromatograph (Thermo Electron Corporation) equipped with a DB-5 capillary column and coupled to a MAT-95X magnetic-sector mass spectrometer. Single-crystal data were acquired with a Bruker APEX II Kappa Duo diffractometer equipped with an APEX II detector at 150 K.

Characterization of 1,6-Bis(2-hydroxyphenyl)-3,4-diphenylhexane-1,6-dione (D1). 1D 1 H and 13 C{ 1 H}, 2D double-quantum-filtered (dqf) COSY, multiplicity-edited HSQC, and HMBC spectra of D1 are shown in Figures S5–S9. 1 H and 13 C{ 1 H} chemical-shift data are summarized as follows: 1 H NMR (500 MHz, chloroform-d): δ 12.15 (s, 1H), 7.66 (dd, J = 8.1, 1.7 Hz, 1H), 7.44 (ddd, J = 8.5, 7.2, 1.7 Hz, 1H), 7.24–7.15 (m, 3H), 6.97 (dd, J = 7.7, 1.8 Hz, 2H), 6.94 (dd, J = 8.5, 1.2 Hz, 1H), 6.86 (ddd, J = 8.1, 7.2, 1.2 Hz, 1H), 3.87 (m, 1H), 3.43–3.38 (m, 2H). 13 C{ 1 H} NMR (126 MHz, chloroform-d): δ 204.7 (s), 162.6 (s), 140.6 (s), 136.5 (d), 129.8 (d), 129.1 (d), 128.2 (d), 127.0 (d), 119.5 (s), 119.0 (d), 118.7 (d), 45.3 (d), 41.4 (t). High-resolution ESI–MS exact mass calcd for C₃₀H₂₅O₃ [M – (H₂O) + H]⁺ 433.1804, found 433.1798. White needle crystal, melting point = 152–153 °C.

The most downfield peak at 204.7 ppm in the ¹³C{¹H} spectrum (Figure S6) is assigned to the carbonyl carbon C1". In the ¹H spectrum (Figure S5), J-coupling patterns of the four ¹H peaks at 7.66, 7.44, 6.94, and 6.86 ppm and the correlations among them in the dqfCOSY spectrum (Figure S7) indicate that these protons belong to the 1,2-disubstituted benzene ring. The proton at 7.66 ppm showed a correlation to the carbonyl carbon in the HMBC spectrum (Figure S9) and is therefore assigned to H6. Consequently, the other three protons at 7.44, 6.94, and 6.86 ppm can be assigned to H4, H3, and H5, respectively. From the HSQC spectrum (Figure S8), these protons are attached to carbons C3 to C6. In the HMBC spectrum, both H4 and H6 protons are correlated with the carbon at 162.6 ppm. This carbon is assigned to C2 based on its chemical shift and the correlations through vicinal CH (${}^{3}J_{CH}$) coupling. In addition, the HMBC spectrum also showed that both H3 and H5 protons are correlated with the carbon at 119.5 ppm; this carbon is assigned to

A single proton signal at 12.15 ppm that shows no correlation to any carbon in the HSQC spectrum, is assigned to the OH proton. In the HMBC spectrum, three strong correlations to C1, C2, and C3, respectively, and one weak correlation to C4, were observed.

In the multiplicity-edited HSQC spectrum (Figure S8), the negative peak (in blue color) is undoubtedly assigned to the methylene group; we assign the methylene proton H2'' correlated to the proton at 3.87 ppm in the dqfCOSY to H3''. Carbon C3'' can be obtained from the HSQC spectrum. For the HMBC spectrum, the carbonyl carbon showed strong correlation to H2'' protons and weak

correlation to the H3" proton, confirming the assignments of this part of the molecule. It should be noted that the two protons of the methylene group are not exactly equivalent; second-order effects were seen for the H2" and H3" peaks in the ¹H spectrum.

Two protons at 6.97 ppm showed a correlation in the HMBC spectrum to carbon C3''. These protons are assigned to H2' and H6'. Their directly attached carbons C2' and C6' can be obtained from the HSQC spectrum. In the dqfCOSY spectrum, protons H2' and H6' showed a correlation to the proton signals at 7.20 ppm. Integration of the proton signals at 7.20 ppm indicated three protons; two were assigned to H3' and H5' and the other to H4'. These three protons are attached to carbons C3', C5', and C4', as can be concluded from the HSQC spectrum. Carbons C3' and C5' are equivalent. Overlapped H3'/H5' and H4' peaks were resolved in the HSQC spectrum. Finally, in the HMBC spectrum, H2'' and H3'' showed correlations to the quaternary carbon at 140.6 ppm; this carbon is assigned to C1'. In addition, these two protons showed correlations to carbons C2'/C6'.

Characterization of (*Z*)-2,2'-(1,2-Diphenylethene-1,2-diyl)-bis(benzofuran-3(2*H*)-one) (D2). 1D 1 H and 13 C{ 1 H}, 2D dqfCOSY, HSQC, and HMBC spectra of D2 are shown in Figures S10–S14. 1 H chemical shift and multiplicity as well as 13 C{ 1 H} chemical shift data are summarized as follows: 1 H NMR (500 MHz, chloroform-*d*): δ 7.99 (d, *J* = 7.5 Hz, 2H), 7.62 (t, *J* = 8.2 Hz, 1H), 7.61 (d, *J* = 7.4 Hz, 1H), 7.42 (t, *J* = 7.5 Hz, 2H), 7.37 (t, *J* = 7.5 Hz, 1H), 7.33 (d, *J* = 8.2 Hz, 1H), 7.13 (t, *J* = 7.4 Hz, 1H). 13 C{ 1 H} NMR (126 MHz, chloroform-*d*): δ 183.3 (s), 165.6 (s), 145.1 (s), 136.6 (d), 135.3 (s), 130.7 (d), 129.5 (d), 128.4 (d), 125.0 (s), 124.6 (d), 123.2 (d), 122.2 (s), 112.9 (d). High-resolution ESI–MS exact mass calcd for C_{30} H₁₈O₄ [M + Na]⁺ 465.1085, found 465.1086. Orange crystal, melting point = 163–164 °C.

Analysis of ¹H-¹H correlations in the dqfCOSY spectrum (Figure S12) as well as *J*-coupling patterns of the ¹H peaks in the ¹H spectrum (Figure S10) revealed the assignments of the three ¹H peaks at 7.99, 7.42, and 7.37 ppm to five protons of the monosubstituted benzene ring. The signal at 7.99 ppm (d, J = 7.5 Hz, 2H) is assigned to H2' and H6', which are equivalent, whereas the signal at 7.42 ppm (t, J =7.5 Hz, 2H) is assigned to H3' and H5' which are equivalent. Finally, the signal at 7.37 ppm (t, J = 7.5 Hz, 1H) is assigned to H4'. Secondorder effects were seen for the H4' as well as H3'/H5'. Analysis of COSY correlations and *J*-coupling patterns also indicated that the four protons at 7.62 (t, J = 8.2 Hz, 1H), 7.61 (d, J = 7.4 Hz, 1H), 7.33 (d, J= 8.2 Hz, 1H), and 7.13 ppm (t, J = 7.4 Hz, 1H), respectively, belong to the 1,2-disubstituted benzene ring. An H6 triplet partially overlaps the H4 doublet in the ¹H spectrum; however, these signals are discernible in the 2D HSQC spectrum and are assigned to C4 and C6. In the ¹³C{¹H} spectrum (Figure S11), the most downfield peak at 183.3 ppm is assigned to the carbonyl carbon C3. In the HMBC spectrum (Figure \$14), the proton at 7.61 ppm showed a correlation to the carbonyl carbon and is assigned to H4. Consequently, the other three protons of the 1,2-disubstituted benzene ring at 7.62, 7.33, and 7.13 ppm can be assigned to H6, H7, and H5, respectively. All CH carbons can be assigned from the HSQC (Figure \$13).

All other quaternary carbons can be assigned from the HMBC spectrum. Both H5 and H7 protons showed correlations to the carbon at 122.2 ppm; this carbon is assigned to C9 based on its chemical shift and from the correlations through vicinal CH (${}^3J_{\rm CH}$) coupling. There is a correlation of H4 and/or H6 protons with the carbon at 165.6 ppm; this carbon is assigned to C8. Due to the overlap of protons H4 and H6, their individual correlations to carbon C8 were not resolved. A weaker correlation between proton H7 and carbon C8 through geminal CH (${}^2J_{\rm CH}$) coupling was also detected. In addition, the HMBC spectrum showed a strong correlation of protons H2′ and H6′ with the carbon at 125.0 ppm; this carbon is assigned to C′. Finally, the last carbon at 145.1 ppm, which did not show a correlation to any proton, is assigned to C2.

Characterization of (*Z*)-1,6-Bis(2-hydroxyphenyl)-3,4-diphenylhex-3-ene-1,6-dione (l2). 1 H NMR (500 MHz, CDCl₃): δ 12.14 (s, 1H, O–H), 7.5 (d, J = 8.3 Hz, 1H, H-2′), 7.39 (t, J = 7.8 Hz, 1H, H-4′), 7.35 (d, J = 7.3 Hz, 2H, H-2″ + H-6″), 7.30 (t, J = 7.7 Hz,

2H, H-3" + H-5''), 7.22 (t, J = 7.3 Hz, 1H, H-4"), 6.91 (d, J = 8.3 Hz, 1H, H-5'), 6.76 (t, J = 7.8 Hz, 1H, H-3'), 4.06 (s, 2H, CH₂). 13 C{ 1 H} NMR (126 MHz, CDCl₃): δ 203.6 (C = O), 162.2 (C-5'a), 141.1 (C-1"), 136.2 (C-4'), 135.5 (C-3), 129.9 (C-2'), 128.6 (C-3'' + C-5''), 128.3 (C-2'' + C-6''), 127.5 (C-4''), 119.3 (C-2'a), 118.7 (C-3'), 118.4 (C-5'), 45.6 (CH₂). High-resolution ESI–MS exact mass calcd for C_{30} H₂₃O₃ [M - H₂O + H]⁺ 431.1675, found 431.1527.

We arrived at the structure of I2 by means of two-dimensional HMBC, COSY, and HSQC NMR experiments (Figure S17-S20). The structure of I2 is very similar to that of D1, except that the two subunits are connected via a C=C bond for I1 instead of a single C-C bond for D1. NMR spectra of I2 are also similar to those of D1. In the ¹³C spectrum, the most deshielded carbon is assigned to the carbonyl carbon C-1. In the HMBC spectrum (Figure S15), an aromatic proton at 7.5 ppm shows a correlation to the carbonyl carbon; this proton is assigned as proton H2'. Protons H2'-H5' and their directly attached carbons (C2'-C5') can be assigned from the COSY (Figure S16) and the HSQC (Figure S17) spectra, respectively. In the COSY spectrum, proton H2' shows a correlation with proton H3', proton H3' shows a correlation with proton H4', and finally, proton H4' shows a correlation with proton H5'. Similarly, from the HSQC spectrum, the directly attached carbons of protons H2' to H5' can be obtained. In the HMBC spectrum, protons H2' and H4' show ³J_{CH} correlations to carbons C4' and C2', respectively, whereas protons H3' and H5' show ³J_{CH} correlations to carbons C5' and C3', respectively. Moreover, data obtained from the HMBC spectrum reveal that both H2' and H4' protons correlate with a carbon signal at 162.2 ppm. This signal is assigned to carbon C5'a on the basis of its chemical shift and from the ${}^{3}J_{\rm CH}$ correlations. In addition, the HMBC spectrum shows that H3' and H5' protons are both correlated with a carbon at 119.3 ppm; this carbon is assigned to

We assigned the proton signal at 4.06 ppm to the methylene protons (H2). Methylene proton H2 shows a correlation in the HMBC spectrum with the carbonyl carbon (C1); it also shows a correlation with two other carbons at 135.5 and 141.1 ppm (Figures S15 and S18). Carbons at 135.5 and 141.1 ppm are assigned to C3 and C1", respectively. In the HMBC spectrum, the two protons at 7.35 ppm show correlation to carbon C3; these two protons are assigned to $H2^{\prime\prime}$ and $H6^{\prime\prime}$; thus, protons $H2^{\prime\prime}$ and $H6^{\prime\prime}$ and their directly attached carbons (see HSQC spectrum in Figure S17) are equivalent. A triplet at 7.22 ppm in the proton spectrum shows a correlation to carbons C2" and C6" in the HMBC spectrum (note that carbons C2" and C6" are equivalent); this triplet is assigned to proton H4". In the proton spectrum, the triplet at 7.30 ppm (which integrates to two protons) shows a correlation to carbon C1" in the HMBC spectrum; this triplet is assigned to protons H3" and H5" which are equivalent.

Similarly, the proton signal at 12.14 ppm is assigned to the OH proton. This assignment is supported by the fact that the proton does not show a correlation to any carbon in the HSQC spectrum, implying that it is not directly bonded to a carbon. It shows three correlations in the HMBC spectrum (Figures S15 and S18), one to the quaternary carbon C5'a and two more to C2'a and C5'. It must be noted that, due to the near overlap of carbons C5' and C2'a, their individual correlations to the OH proton are not resolved in the HMBC spectrum.

Computational Analysis. Electronic structure calculations were performed with the aid of the Gaussian (G16) package. We optimized geometries using B3LYP density functional $^{46-48}$ with 6-31+G(d,p) $^{49-52}$ basis set. The solvent environment was modeled with SMD-SCRF⁵³ implicit solvation model for acetonitrile as solvent (ε = 35.688), included in all geometry optimizations. Optimized geometries were confirmed as minima on the potential energy surface by vibrational frequency calculations with no imaginary frequency. Transition states had with only one imaginary frequency with a transition vector leading from reactant to the product. Transition states were further validated using the intrinsic reaction coordinate (IRC) calculations. Thermal and entropy contribution to the Gibbs free energy was calculated by the use of unscaled B3LYP frequencies

and rigid rotor/harmonic oscillator approximations at 298.15 K. For molecules with multiple rotatable bonds, a conformational search was performed with the aid of the LowModeMD module⁵⁴ implemented in the molecular operating environment (MOE, version 2018.01) with Amber2010:EHT force field.⁵⁵ We further refined structures with energies lower than 5 kcal/mol by performing geometry optimization at the B3LYP/6-31+G(d,p) level of theory in acetonitrile, and the lowest energy structure was used for further analysis.

For a reaction, $X_{(sol)} + ne^-_{(sol)} \rightarrow X^{n-}_{(sol)}$, the standard reduction potential, $E^o_{(sol)}$ is given by

$$E_{(\text{sol})}^{\,o} = -\frac{\Delta G_{(\text{sol})}^{*}}{nF} - \text{SCE}$$

where $\Delta G_{(sol)}^* = G_{X,(sol)}^* - G_{X^{n},(sol)}^* - G_{e,(g)}^*$ is the standard free-energy change for a redox reaction in acetonitrile and $G_{e,(g)}^* = -0.87$ kcal/mol is the gas-phase free energy of the electron at 298.15 K obtained from the literature. The faraday (F) is 23.06 kcal/(mol-V), and n is the number of electrons, with SCE being the absolute potential of the standard calomel electrode (4.43 V). For reactions involving proton-coupled electron transfer, the free energy of a proton in acetonitrile was calculated from the relation

$$G^*_{\mathrm{H}^+,(\mathrm{sol})} = G^{\,\mathrm{o}}_{\mathrm{H}^+,(\mathrm{g})} + \Delta G^*_{\mathrm{solv},(\mathrm{sol})} + \Delta G^{\mathrm{latm} \to 1\mathrm{M}}$$

where $G^{\rm o}_{{
m H}^+,({
m g})}=-6.29$ kcal/mol at 298.15 K is derived from $G^{\rm o}_{{
m H}^+,({
m g})}=H^{\rm o}_{({
m g})}-TS^{\rm o}_{({
m g})}$, with $H^{\rm o}_{({
m g})}=1.48$ kcal/mol, $S^{\rm o}_{({
m g})}=26.05$ cal/(mol·K), $\Delta G^*_{{
m solv},(acetonitrile)}=-260.5$ kcal/mol is the solvation energy of the proton taken from the literature, 58 and $\Delta G^{{
m lat} m \to 1M}=1.89$ kcal/mol is the correction to the free energy for changing from the standard state of 1 atm to 1 M. 59

ASSOCIATED CONTENT

5 Supporting Information

The Supporting Information is available free of charge at https://pubs.acs.org/doi/10.1021/acs.joc.0c01220.

X-ray data for D1 (CIF)

X-ray data for D2 (CIF)

Copies of ¹H NMR and ¹³C NMR spectra for new compounds, X-ray diffraction data (PDF)

AUTHOR INFORMATION

Corresponding Author

Mohammad S. Mubarak — Department of Chemistry, Indiana University, Bloomington, Indiana 47405, United States; Department of Chemistry, The University of Jordan, Amman 11942, Jordan; ⊚ orcid.org/0000-0002-9782-0835; Email: mmubarak@indiana.edu, mmubarak@ju.edu.jo

Authors

Seyyedamirhossein Hosseini — Department of Chemistry, Indiana University, Bloomington, Indiana 47405, United States; © orcid.org/0000-0002-3521-1062

Bishnu Thapa — Department of Chemistry, Indiana University, Bloomington, Indiana 47405, United States; ⊙ orcid.org/ 0000-0003-3521-1062

Maria J. Medeiros — Departamento de Química, Universidade do Minho, 4710-057 Braga, Portugal

Erick M. Pasciak – Department of Chemistry, Indiana University, Bloomington, Indiana 47405, United States

Michael A. Pence – Department of Chemistry, Indiana University, Bloomington, Indiana 47405, United States

Eric B. Twum – Department of Chemistry, Indiana University, Bloomington, Indiana 47405, United States

Jonathan A. Karty – Department of Chemistry, Indiana University, Bloomington, Indiana 47405, United States **Xinfeng Gao** – Department of Chemistry, Indiana University, Bloomington, Indiana 47405, United States

Krishnan Raghavachari — Department of Chemistry, Indiana University, Bloomington, Indiana 47405, United States; orcid.org/0000-0003-3275-1426

Dennis G. Peters — Department of Chemistry, Indiana University, Bloomington, Indiana 47405, United States; orcid.org/0000-0002-3716-8355

Complete contact information is available at: https://pubs.acs.org/10.1021/acs.joc.0c01220

Notes

The authors declare no competing financial interest. Prof. Dennis G. Peters passed away on April 13, 2020.

ACKNOWLEDGMENTS

K.R. acknowledges financial support from the National Science Foundation (NSF) (Grant No. CHE-1665427).

REFERENCES

- (1) Nijveldt, R. J.; van Nood, E.; van Hoorn, D. E. C.; Boelens, P. G.; van Norren, K.; van Leeuwen, P. A. M. Flavonoids: A Review of Probable Mechanisms of Action and Potential Applications. *Am. J. Clin. Nutr.* **2001**, *74*, 418–425.
- (2) Panche, A. N.; Diwan, A. D.; Chandra, S. R. Flavonoids: An Overview. J. Nutr. Sci. 2016, 5, 1–15.
- (3) Chen, A. Y.; Adamek, R. N.; Dick, B. L.; Credille, C. V.; Morrison, C. N.; Cohen, S. M. Targeting Metalloenzymes for Therapeutic Intervention. *Chem. Rev.* **2019**, *119*, 1323–1455.
- (4) Li, Y.; Shibahara, A.; Matsuo, Y.; Tanaka, T.; Kouno, I. Reaction of the Black Tea Pigment Theaflavin during Enzymatic Oxidation of Tea Catechins. *J. Nat. Prod.* **2010**, *73*, 33–39.
- (5) Olleik, H.; Yahiaoui, S.; Roulier, B.; Courvoisier-Dezord, E.; Perrier, J.; Pérès, B.; Hijazi, A.; Baydoun, E.; Raymond, J.; Boumendjel, A.; Maresca, M.; Haudecoeur, R. Aurone Derivatives as Promising Antibacterial Agents against Resistant Gram-positive Pathogens. *Eur. J. Med. Chem.* **2019**, *165*, 133–141.
- (6) Jeong, K.-W.; Lee, J.-Y.; Kang, D.-II.; Lee, J.-U.; Shin, S. Y.; Kim, Y. Screening of Flavonoids as Candidate Antibiotics against Enterococcus faecalis. *J. Nat. Prod.* **2009**, *72*, 719–724.
- (7) Groweiss, A.; Cardellina, J. H.; Boyd, M. R. HIV-Inhibitory Prenylated Xanthones and Flavones from Maclura tinctoria. *J. Nat. Prod.* **2000**, *63*, 1537–1539.
- (8) Asada, Y.; Li, W.; Yoshikawa, T. The First Prenylated Biaurone, Licoagrone from Hairy Root Cultures of Glycyrrhiza glabra. *Phytochemistry* **1999**, *50*, 1015–1019.
- (9) Pillaiyar, T.; Namasivayam, V.; Manickam, M.; Jung, S.-H. Inhibitors of Melanogenesis: An Updated Review. *J. Med. Chem.* **2018**, *61*, 7395–7418.
- (10) Alsayari, A.; Muhsinah, A. B.; Hassan, M. Z.; Ahsan, M. J.; Alshehri, J. A.; Begum, N. Aurone: A Biologically Attractive Scaffold as Anticancer Agent. *Eur. J. Med. Chem.* **2019**, *166*, 417–431.
- (11) Lucas, S. D.; Carrasco, M. P.; Goncalves, L. M.; Moreira, R.; Guedes, R. C. Discovery of C-shaped Aurone Human Neutrophil Elastase Inhibitors. *MedChemComm* **2015**, *6*, 1508–1512.
- (12) Haudecoeur, R.; Ahmed-Belkacem, A.; Yi, W.; Fortuné, A.; Brillet, R.; Belle, C.; Nicolle, E.; Pallier, C.; Pawlotsky, J.-M.; Boumendjel, A. Discovery of Naturally Occurring Aurones That Are Potent Allosteric Inhibitors of Hepatitis C Virus RNA-Dependent RNA Polymerase. *J. Med. Chem.* **2011**, *54*, 5395–5402.
- (13) Okombi, S.; Rival, D.; Bonnet, S.; Mariotte, A.-M.; Perrier, E.; Boumendjel, A. Discovery of Benzylidenebenzofuran-3(2H)-one (Aurones) as Inhibitors of Tyrosinase Derived from Human Melanocytes. *J. Med. Chem.* **2006**, *49*, 329–333.
- (14) Ni, H.; Yu, Z.; Yao, W.; Lan, Y.; Ullah, N.; Lu, Y. Catalyst-controlled Regioselectivity in Phosphine Catalysis: The Synthesis of

- Spirocyclic Benzofuranones via Regiodivergent [3 + 2] Annulations of Aurones and an Allenoate. *Chem. Sci.* **2017**, *8*, 5699–5704.
- (15) Wang, Z.-P.; Xiang, S.; Shao, P.-L.; He, Y. Catalytic Asymmetric [3 + 2] Cycloaddition Reaction between Aurones and Isocyanoacetates: Access to Spiropyrrolines via Silver Catalysis. *J. Org. Chem.* **2018**, *83*, 10995–11007.
- (16) Chen, K.-Q.; Gao, Z.-H.; Ye, S. Bifunctional N-heterocyclic Carbene Catalyzed [3 + 4] Annulation of Enals with Azadienes: Enantioselective Synthesis of Benzofuroazepinones. *Org. Chem. Front.* **2019**, *6*, 405–409.
- (17) Gao, Z.-H.; Chen, K.-Q.; Zhang, Y.; Kong, L.-M.; Li, Y.; Ye, S. Enantioselective Heterocyclic Carbene-Catalyzed Synthesis of Spirocyclic Oxindole-benzofuroazepinones. *J. Org. Chem.* **2018**, 83, 15225–15235.
- (18) Yatabe, T.; Jin, X.; Mizuno, N.; Yamaguchi, K. Unusual Olefinic C–H Functionalization of Simple Chalcones Toward Aurones Enabled by the Rational Design of a Function-Integrated Heterogeneous Catalyst. ACS Catal. 2018, 8, 4969–4978.
- (19) Chang, M.-Y.; Chen, H.-Y.; Tsai, Y.-L. Temperature-Controlled Desulfonylative Condensation of α -Sulfonyl o-Hydroxyacetophenones and 2-Formyl Azaarenes: Synthesis of Azaaryl Aurones and Flavones. *J. Org. Chem.* **2019**, 84, 326–337.
- (20) Harkat, H.; Blanc, A.; Weibel, J.-M.; Pale, P. Versatile and Expeditious Synthesis of Aurones via AuI-Catalyzed cyclization. *J. Org. Chem.* **2008**, *73*, 1620–1623.
- (21) Weng, Y.; Chen, Q.; Su, W. copper-Catalyzed Intermolecular Tandem Reaction of (2-Halogenphenyl)(3-phenyloxiran-2-yl)-methanones: Synthesis of (Z)-Aurones. *J. Org. Chem.* **2014**, *79*, 4218–4224.
- (22) Qi, X.; Li, R.; Wu, X.-F. Selective Palladium-Catalyzed Carbonylative Synthesis of Auron with Formic Acid as the CO source. *RSC Adv.* **2016**, *6*, 62810–62813.
- (23) Zwergel, C.; Valente, S.; Salvato, A.; Xu, Z.; Talhi, O.; Mai, A.; Silva, A.; Altucci, L.; Kirsch, G. Novel Benzofuran—chromone and —coumarin Derivatives: Synthesis and Biological Activity in K562 Human Leukemia Cells. *MedChemComm* **2013**, *4*, 1571–1579.
- (24) Chen, Z.; Wang, B.; Zhang, J.; Yu, W.; Liu, Z.; Zhang, Y. Transition Metal-catalyzed C—H Bond Functionalizations by the Use of Diverse Directing Groups. *Org. Chem. Front.* **2015**, *2*, 1107—1295.
- (25) Carrasco, M. P.; Newton, A. S.; Gonçalves, L.; Góis, A.; Machado, M.; Gut, J.; Nogueira, F.; Hänscheid, T.; Guedes, R. C.; dos Santos, D. J. V. A.; Rosenthal, P. J.; Moreira, R. Probing the Aurone Scaffold against Plasmodium falciparum: Design, Synthesis and Antimalarial Activity. Eur. J. Med. Chem. 2014, 80, 523–534.
- (26) Jiang, Y.; Xu, K.; Zeng, C. Use of Electrochemistry in the Synthesis of Heterocyclic Structures. *Chem. Rev.* **2018**, *118*, 4485–4540
- (27) Du, P.; Brosmer, J. L.; Peters, D. G. Electrosynthesis of Substituted 1*H*-Indoles from *o*-Nitrostyrenes. *Org. Lett.* **2011**, *13*, 4072–4075.
- (28) Hosseini, S.; Bawel, S. A.; Mubarak, M. S.; Peters, D. G. Rapid and High-Yield Electrosynthesis of Benzisoxazole and Some Derivatives. *ChemElectroChem* **2019**, *6*, 4318–4324.
- (29) Horn, E. J.; Rosen, B. R.; Baran, P. S. Synthetic Organic Electrochemistry: An Enabling and Innately Sustainable Method. *ACS Cent. Sci.* **2016**, *2*, 302–308.
- (30) Yan, M.; Kawamata, Y.; Baran, P. S. Synthetic Organic Electrochemical Methods Since 2000: On the Verge of a Renaissance. *Chem. Rev.* **2017**, *117*, 13230–13319.
- (31) Bard, A. J.; Faulkner, L. R. Electrochemical Methods: Fundamentals and Applications, 2nd ed.; Wiley: New York, 2001.
- (32) Francke, R.; Quell, T.; Wiebe, A.; Waldvogel, S. R. Oxygen-Containing Compounds: Alcohols, Ethers, and Phenols. In *Organic Electrochemistry* 5th ed.; Hammerich, O., Speiser, B., Eds.; CRC Press: Boca Raton, FL, 2016; pp 981–1033.
- (33) Zimmer, J. P.; Richards, J. A.; Turner, J. C.; Evans, D. H. Electrochemical Reduction of α,β -Unsaturated Ketones. *Anal. Chem.* **1971**, 43, 1000–1006.

- (34) Moncelli, M. R.; Nucci, L.; Mariani, P.; Guidelli, R. The Mechanism of Electrohydrodimerization of Chalcone on Mercury from Aqueous Solutions. *J. Electroanal. Chem. Interfacial Electrochem.* 1985, 183, 285–302.
- (35) Brillas, E.; Ortíz, A. Electrohydrodimerization of 2-Cyclohexen-1-one in Hydroethanolic Medium. *Electrochim. Acta* **1985**, *30*, 1185–1190.
- (36) Bastida, R. M.; Brillas, E.; Costa, J. M. Electrohydrodimerization of α , β -Unsaturated Alicyclic and Aliphatic Ketones in Hydroethanolic Solutions on a Mercury Electrode: I. Reduction of 2-Cyclopenten-1-one. *J. Electrochem. Soc.* **1991**, *138*, 2289–2296.
- (37) Pasciak, E. M.; Rittichier, J. T.; Chen, C.-H.; Mubarak, M. S.; VanNieuwenhze, M. S.; Peters, D. G. Electroreductive Dimerization of Coumarin and Coumarin Analogues at Carbon Cathodes. *J. Org. Chem.* **2015**, *80*, 274–280.
- (38) Vieira, K. L.; Peters, D. G. Voltammetric Behavior of Tertiary Butyl Bromide at Mercury Electrodes in Dimethylformamide. *J. Electroanal. Chem. Interfacial Electrochem.* **1985**, *196*, 93–104.
- (39) Dahm, C. E.; Peters, D. G. Catalytic Reduction of Iodoethane and 2-Iodopropane at Carbon Electrodes Coated with Anodically Polymerized Films of Nickel(II) Salen. *Anal. Chem.* **1994**, *66*, 3117–3123.
- (40) Vanalabhpatana, P.; Peters, D. G. Catalytic Reduction of 1,6-Dihalohexanes by Nickel(I) Salen Electrogenerated at Glassy Carbon Cathodes in Dimethylformamide. *J. Electrochem. Soc.* **2005**, *152*, E222–E229.
- (41) Cleary, J. A.; Mubarak, M. S.; Vieira, K. L.; Anderson, M. R.; Peters, D. G. Electrochemical Reduction of Alkyl Halides at Vitreous Carbon Cathodes in Dimethylformamide. *J. Electroanal. Chem. Interfacial Electrochem.* 1986, 198, 107–124.
- (42) Marple, L. W. Reference Electrode for Anhydrous Dimethylformamide. *Anal. Chem.* **1967**, *39*, 844–846.
- (43) Manning, C. W.; Purdy, W. C. Reference Electrode for Electrochemical Studies in Dimethylformamide. *Anal. Chim. Acta* **1970**, *51*, 124–126.
- (44) Hall, J. L.; Jennings, P. W. Modification of the Preparation of a Cadmium Amalgam Reference Electrode for Use in *N. Anal. Chem.* 1976, 48, 2026–2027.
- (45) Frisch, M. J. T. G. W.; Schlegel, H. B.; Scuseria, G. E.; Robb, M. A.; Cheeseman, J. R.; Scalmani, G.; Barone, V.; Petersson, G. A.; Nakatsuji, H.; Li, X.; Caricato, M.; Marenich, A. V.; Bloino, J.; Janesko, B. G.; Gomperts, R.; Mennucci, B.; Hratchian, H. P.; Ortiz, J. V.; Izmaylov, A. F.; Sonnenberg, J. L.; Williams-Young, D.; Ding, F.; Lipparini, F.; Egidi, F.; Goings, J.; Peng, B.; Petrone, A.; Henderson, T.; Ranasinghe, D.; Zakrzewski, V. G.; Gao, J.; Rega, N.; Zheng, G.; Liang, W.; Hada, M.; Ehara, M.; Toyota, K.; Fukuda, R.; Hasegawa, J.; Ishida, M.; Nakajima, T.; Honda, Y.; Kitao, O.; Nakai, H.; Vreven, T.; Throssell, K.; Montgomery, J. A., Jr.; Peralta, J. E.; Ogliaro, F.; Bearpark, M. J.; Heyd, J. J.; Brothers, E. N.; Kudin, K. N.; Staroverov, V. N.; Keith, T. A.; Kobayashi, R.; Normand, J.; Raghavachari, K.; Rendell, A. P.; Burant, J. C.; Iyengar, S. S.; Tomasi, J.; Cossi, M.; Millam, J. M.; Klene, M.; Adamo, C.; Cammi, R.; Ochterski, J. W.; Martin, R. L.; Morokuma, K.; Farkas, O.; Foresman, J. B.; Fox, D. J. Gaussian 16, Revision A.03; Gaussian, Inc.: Wallingford, CT, 2016.
- (46) Becke, A. D. Density-functional Thermochemistry. I. The Effect of the Exchange-only Gradient Correction. *J. Chem. Phys.* **1992**, *96*, 2155–2160.
- (47) Becke, A. D. Density-functional Thermochemistry. V. Systematic Optimization of Exchange-correlation Functionals. *J. Chem. Phys.* **1997**, *107*, 8554–8560.
- (48) Lee, C.; Yang, W.; Parr, R. G. Development of the Colle-Salvetti Correlation-energy Formula into a Functional of the Electron Density. *Phys. Rev. B: Condens. Matter Mater. Phys.* **1988**, *37*, 785.
- (49) Francl, M. M.; Pietro, W. J.; Hehre, W. J.; Binkley, J. S.; Gordon, M. S.; DeFrees, D. J.; Pople, J. A. Self-consistent molecular orbital methods. XXIII. A Polarization-type Basis Set for Second-row Elements. *J. Chem. Phys.* **1982**, *77*, 3654–3665.

- (50) Hariharan, P. C.; Pople, J. A. The Influence of Polarization Functions on Molecular Orbital Hydrogenation Energies. *Theoret. Chim. Acta* 1973, 28, 213–222.
- (51) Hehre, W. J.; Ditchfield, R.; Pople, J. A. Self-consistent Molecular Orbital Methods. XII. Further Extensions of Gaussian-type Basis Sets for Use in Molecular Orbital Studies of Organic Molecules. *J. Chem. Phys.* **1972**, *56*, 2257–2261.
- (52) Hehre, W. J.; Ditchfield, R.; Radom, L.; Pople, J. A. Molecular Orbital Theory of the Electronic Structure of Organic Compounds. V. Molecular Theory of Bond Separation. J. Am. Chem. Soc. 1970, 92, 4796–4801.
- (53) Marenich, A. V.; Cramer, C. J.; Truhlar, D. G. Universal Solvation Model Based on Solute Electron Density and on a Continuum Model of the Solvent Defined by the Bulk Dielectric Constant and Atomic Surface Tensions. *J. Phys. Chem. B* **2009**, *113*, 6378–6396.
- (54) Labute, P. LowModeMD—Implicit Low-Mode Velocity Filtering Applied to Conformational Search of Macrocycles and Protein Loops. *J. Chem. Inf. Model.* **2010**, *50*, 792—800.
- (55) Molecular operating environment (MOE); Chemical Computing Group: Montreal, QC, 2018.
- (56) Thapa, B.; Schlegel, H. B. Calculations of pK_as and Redox Potentials of Nucleobases with Explicit Waters and Polarizable Continuum Solvation. *J. Phys. Chem. A* **2015**, *119*, 5134–5144.
- (57) Isse, A. A.; Gennaro, A. Absolute Potential of the Standard Hydrogen Electrode and the Problem of Interconversion of Potentials in Different Solvents. *J. Phys. Chem. B* **2010**, *114*, 7894–7899.
- (58) Rossini, E.; Knapp, E. W. Proton Solvation in Protic and Aprotic Solvents. J. Comput. Chem. 2016, 37, 1082–1091.
- (59) Ben-Naim, A.; Marcus, Y. Solvation Thermodynamics of Nonionic Solutes. *J. Chem. Phys.* **1984**, *81*, 2016–2027.

■ NOTE ADDED AFTER ASAP PUBLICATION

A partially corrected version was published on August 3, 2020; the fully corrected version was reposted on August 6, 2020.